Membrane Binding of pH-Sensitive Influenza Fusion Peptides. Positioning, Configuration, and Induced Leakage in a Lipid Vesicle Model†

Elin K. Esbjörner,*,‡,§ Kamila Oglęcka,§,|| Per Lincoln,‡ Astrid Gräslund,|| and Bengt Nordén*,‡

Department of Chemical and Biological Engineering/Physical Chemistry, Chalmers University of Technology, Kemivägen 10, SE-412 96 Gothenburg, and Department of Biochemistry and Biophysics, The Arrhenius Laboratories, Stockholm University, SE-106 91 Stockholm, Sweden

Received June 2, 2007; Revised Manuscript Received August 22, 2007

ABSTRACT: pH-sensitive HA2 fusion peptides from influenza virus hemagglutinin have potential as endosomal escape-inducing components in peptide-based drug delivery. Polarized light spectroscopy and tryptophan fluorescence were used to assess the conformation, orientation, effect on lipid order, and binding kinetics of wild-type peptide HA2(1−23) and a glutamic acid-enriched analogue (INF7) in large unilamellar POPC or POPC/POPG (4:1) lipid vesicles (LUVs). pH-sensitive membrane leakage was established for INF7 but not HA2(1−23) using an entrapped-dye assay. A correlation is indicated between leakage and a low degree of lipid chain order (assessed by linear dichroism, LD, of the membrane orientation probe retinoic acid). Both peptides display poor alignment in zwitterionic POPC LUVs compared to POPC/POPG (4:1) LUVs, and it was found that peptide−lipid interactions display slow kinetics (hours), resulting in reduced lipid order and increased tryptophan shielding. At pH 7.4, INF7 displays tryptophan emission and LD features indicative of a surface-orientated peptide, suggesting that its N-terminal glutamic acid residues prevent deep penetration into the hydrocarbon core. At pH 5.0, INF7 displays weaker LD signals, indicating poor orientation, possibly due to aggregation. By contrast, the orientation of the HA2(1−23) peptide backbone supports previously reported oblique insertion (∼60−65° relative to the membrane normal), and aromatic side-chain orientations are consistent with an interfacial (pH-independent) location of the C-terminus. We propose that a conformational change upon reduction of pH is limited to minor rearrangements of the peptide "hinge region" around Trp14 and repositioning of this residue.

Peptide-based drug delivery vectors, named cell-penetrating peptides (CPPs)[1] or protein transduction domains (PTDs), have emerged as promising efficient and nontoxic tools in enhancing intracellular delivery of cargo molecules ranging from small organic compounds and small oligonucleotides to larger proteins, plasmid DNA, liposomes, and nanoparticles (*1*). While these vectors were originally thought to deliver cargo into cells via direct membrane penetration mechanisms, it has become increasingly clear that uptake of peptide−cargo constructs is in fact mainly occurring via endocytotic pathways (*2*−*4*). However, since cargo molecules evidently can induce the desired biological effect inside cells (*5*), the peptide−cargo constructs must have a certain capability to escape from endosomes before lysosomal degradation. Since CPPs such as penetratin (pAntp) and Tat peptides are already functional for internalizing cargo via endocytosis, a natural step forward in the development of more efficient peptide-based vectors would be to improve endosomal escape characteristics of peptide−cargo constructs. There are several examples in the literature of strategies to enhance escape from endosomes, all based on utilizing the acidification process that brings down the pH inside the endosome from the physiological 7.4 to around 5 to selectively destabilize endosomal membranes (see ref *6* for a recent review).

The influenza virus is an archetypical example of a virus that uses endosome acidification to enter the cytoplasm. This process has been extensively explored, and the escape mechanism is by membrane fusion, initiated at low pH due to conformational changes in the viral hemagglutinin membrane protein HA2, resulting in exposure of its 20−25 amino acid long N-terminal pH-sensitive and membrane-disruptive segment. This segment is thought to constitute an individually folded domain and has been named simply the fusion peptide due to its ability to mediate fusion of lipid vesicles on its own, even in the absence of the rest of the protein. Comparison of fusion peptide sequences in various subtypes of influenza virus A strains reveals that the sequence is highly

† This work was funded by grants to B.N. and A.G. from the Swedish Cancer Foundation (Cancerfonden) and by grants to B.N. from the European Commission (Sequence-Specific Oligomers for In Vivo Gene Repair, Contract No. 005204, and ZNIP Contract No. 037783).

* To whom correspondence should be addressed. (E.K.E.) E-mail: eline@chalmers.se. Phone: +46(0)31-7723857. (B.N.) E-mail: norden@chalmers.se. Phone: +46(0)31-7723041. Fax: +46(0)31-7723858.

‡ Chalmers University of Technology.

§ These authors contributed equally to this work.

|| Stockholm University.

[1] Abbreviations: ANTS, 8-aminonaphthalene-1,3,6-trisulfonic acid; Asp, aspartic acid; CD, circular dichroism; CPP, cell-penetrating peptide; DPC, dodecylphosphocholine; DPX, *p*-xylene bis(pyridinium bromide); Glu, glutamic acid; LD, linear dichroism; LUV, large unilamellar vesicle; POPC, 1-palmitoyl-2-oleoyl-*sn*-glycero-3-phosphatidylcholine; POPG, 1-palmitoyl-2-oleoyl-*sn*-glycero-3-phosphatidyl-*rac*-glycerol; PTD, protein transduction domain; Trp, tryptophan; Tyr, tyrosine.

10.1021/bi701075y CCC: $37.00
Published on Web 11/01/2007

Table 1: Amino Acid Sequences of HA2(1−23) and INF7[a]

peptide	sequence
HA2(1−23)	Ac-G-L-F-G-A-I-A-G-F-I-*E*-N-G-**W**-*E*-G-M-I-*D*-G-**W**-**Y**-G-NH_2
INF7	Ac-G-L-F-*E*-A-I-*E*-G-F-I-*E*-N-G-**W**-*E*-G-M-I-*D*-G-**W**-**Y**-G-NH_2

[a] Aromatic residues are marked in bold and acidic residues in italics. The peptides were synthesized with an acetylated N-terminus and an amidated C-terminus.

conserved (*7*). It is believed that pH sensitivity of this peptide is a result of the inability to form a stable α-helix upon membrane binding at neutral pH due to electrostatic repulsion between the negatively charged residues Glu11, Glu15, and Asp19. Several attempts have been made to improve pH sensitivity by introducing additional glutamic acid residues in the N-terminal part of HA2 (*8*, *9*).

The structure of a fusion peptide corresponding to residues 1−20, HA2(1−20), bound to DPC micelles has been determined by NMR at both physiological (pH 7.4) and endosomal (pH 5) conditions (*10*). The peptide was concluded to bind to the micelles in a crescent-shaped fashion, with the N-terminal part forming an α-helix that penetrates into the micelle core in a tilted (oblique) conformation. Oblique insertion angles of HA2 peptides have also been suggested from polarized infrared spectroscopy studies on supported lipid bilayers as well as from EPR spectroscopy studies with spin-labeled peptides associated with lipid vesicle membranes (*10*, *11*). In addition to the oblique insertion, HA2 fusion peptides are thought to form a hinge at Gly11 and Asn12 which is stabilized by hydrogen bonds, and this structure has been concluded essential for biological activity (*12*). In the above-mentioned NMR model the C-terminal part of HA2(1−20) is seemingly unstructured at pH 7.4 but adopts a short 3_{10} helix at pH 5. The "hinge region" creates a hydrophobic pocket in which Trp14 is positioned and which is thought to aid in membrane destabilization by imposing negative curvature on the membrane. A similar structure has been observed for a glutamic acid-enriched peptide (E5), also in DPC micelles (*13*).

Whereas membrane fusion is a viable endosomal escape strategy for viruses as well as for drug delivery using liposomes or even lipoplexes, membrane fusion may not be applicable in increasing endosomal escape of CPP−cargo constructs. However, in addition to promoting membrane fusion, HA2 peptides do act destabilizing on liposomal membranes as well as erythrocytes, which results in leakage of the entrapped content (*9*, *14*, *15*). Therefore, their utility in promoting endosomal escape of non-lipid-based delivery systems has been tested (*9*). Particularly for peptide-based drug delivery the concept of using a pH-sensitive peptide segment that can be fused to a cell-penetrating peptide using automated peptide synthesis is an attractive approach for enhancing delivery of cargo to the cytosol. A proof-of-principle for this strategy has already been demonstrated using a Tat−HA2 peptide for delivery of a Tat−Cre fusion protein (*5*).

We have studied the binding geometry, degree of orientation, membrane association, and membrane-disruptive properties of a wild-type HA2 fusion peptide (residues 1−23 in the HA2 protein of influenza virus strain X-31 (H3N2)) and a suggestively more pH-sensitive mutant (denoted INF7) enriched in glutamic acid residues in the N-terminal part (see Table 1 for the sequences) (*9*) using polarized light spectroscopy (flow linear dichroism and circular dichroism) and fluorescence spectroscopy techniques. Large unilamellar vesicles (LUVs) with a diameter of 100 nm composed of synthetic phospholipids were used as membrane models. As mentioned, the fusion activity of HA peptides has already been extensively explored in several contexts. Moreover, the enhancement of endosomal escape in peptide-based drug delivery will not involve fusion events, but rather be a consequence of the general membrane-destabilizing properties of the peptide construct. Therefore, this study was undertaken to explore structure−activity relationships for these peptides in the context of membrane disruption, and all experiments have been performed under conditions where we observe significant leakage of entrapped dyes from LUVs.

From binding geometries and the degree of alignment as well as the effects of the lipid chain order and positioning of aromatic tryptophan residues, we have been able to pinpoint differences between wild-type HA2(1−23) and the glutamic acid-enriched analogue INF7, important for the understanding of their membrane-disruptive characteristics. In addition, the binding geometry of the HA2(1−23) backbone and aromatic residues, obtained here from linear dichroism experiments, will be compared to existing NMR models for slightly shorter HA2(1−20), and the positioning of the C-terminal part of HA2 peptides will be discussed.

MATERIALS AND METHODS

Materials. Peptides (>90% purity) were purchased from NeoMPS (Strasbourg, France) and dissolved at high concentration (up to 1 mM) in 0.1 M bicarbonate/acetonitrile/H_2O (1:1:2). Peptide stock solutions were kept frozen or on ice. Lipids (1-palmitoyl-2-oleoyl-*sn*-glycero-3-phosphatidylcholine (POPC) and 1-palmitoyl-2-oleoyl-*sn*-glycero-3-phosphatidyl-*rac*-glycerol (POPG)) were purchased from Larodan (Malmö, Sweden). Buffer chemicals (sodium phosphate salts and citrate) were from Fluka. Sucrose, 8-aminonaphthalene-1,3,6-trisulfonic acid (ANTS), and *p*-xylene bis(pyridinium bromide) (DPX) were from Sigma. The buffers were 10 mM sodium phosphate for pH 7.4 conditions and 10 mM sodium citrate/sodium phosphate for pH 5.0. Deionized water from a Millipore system was used. In all linear dichroism experiments 50% (w/w) sucrose was dissolved in the buffer to reduce light scattering from the LUVs (vide infra).

Large Unilamellar Vesicle Preparation. LUVs were prepared by mixing appropriate amounts of lipids, dissolved in chloroform in a round-bottom flask, and thereafter removing the solvent by rotary evaporation. Remaining trace amounts of solvent were removed by placing the lipid film under vacuum for at least 2 h. Thereafter the lipid film was dissolved in the appropriate buffer by vortexing. The lipid suspension was subjected to five freeze−thaw cycles and thereafter extruded 21 times through polycarbonate filters

with a pore size of 100 nm using a Liposofast pneumatic extruder or a hand-held syringe extruder (Avestin, Canada). The lipid vesicles used were composed of either 100% POPC or POPC/POPG at a molar ratio of 4:1 (20% negative charge).

Circular Dichroism. Circular dichroism (CD) was used to examine the secondary structure of HA2(1−23) and INF7 in buffer and bound to LUVs (POPC or POPC/POPG (4:1)) at pH 7.4 and 5.0. Spectra were recorded between 190 and 260 nm in 1 nm increments on a JASCO J-810 spectropolarimeter at 25 °C using a scan speed of 50 nm/min and a band-pass of 2 nm. A total of 20 scans were recorded and averaged by the computer. Spectra were corrected for background contributions by subtracting appropriate blanks. The path length of the quartz cell was 1 mm. The peptide-to-lipid molar ratio was 1:50, and the peptide concentration was 10 μM. The method of Chen et al. (*16*) was used to estimate the fraction of peptide that adopts α-helical conformation from the mean molar residue ellipticity, $[\theta]_{MR}$, at 222 nm according to

$$X_{helix} = \frac{[\theta]_{MR,222nm}}{-39500 \times (1 - 2.57/n)} \quad (1)$$

with n the number of residues in the peptide.

Linear Dichroism. Linear dichroism (LD) is the differential absorption of linearly polarized light parallel and perpendicular to an orientation axis (eq 2) and requires a macroscopically aligned sample. Liposomes can be deformed by shear flow in a rotating Couette cell device, resulting in slightly ellipsoidal vesicles which align in the flow (*17*). Peptides that bind to the lipid surface in a nonrandom fashion will hence also be aligned, and their transition moments will exhibit LD in the 190−300 nm spectral region. Information on the binding geometry can be obtained by normalizing the LD spectrum with respect to the isotropic absorption (A_{iso}). The normalized LD is thus a path length- and concentration-independent quantity and is called reduced LD (LD^r). For a nonoverlapping transition moment, the relation between LD^r and its angle relative to the membrane normal (the only unique axis in a membrane system) is given by

$$LD(\lambda) = A_{II}(\lambda) - A_{\perp}(\lambda) \quad (2)$$

$$LD^r = \frac{LD}{A_{iso}} = \frac{3}{4}S(1 - 3\cos^2\alpha) \quad (3)$$

with S the macroscopic orientation parameter describing the ordering of the sample. S can vary between 0 and 1, with the latter denoting a perfectly aligned sample.

Linear dichroism was measured using a JASCO J-720 spectropolarimeter equipped with an Oxley prism to obtain linearly polarized light (*18*). The samples were oriented in an outer-rotating Couette cell with a total light path of 1 mm under a shear rate of 3100 s^{-1}. Spectra were recorded from 190 to 500 nm using a scan speed of 100 nm/min and a band-pass of 2 nm. Three successive scans were recorded and averaged by the computer. Spectra were corrected for background contributions by subtracting a spectrum that was collected without rotation of the Couette cell (isotropic sample). To reduce light scattering from the lipid vesicles and to improve the macroscopic orientation, 50% (w/w) sucrose buffer was used in all LD experiments. The sucrose buffer matches the refractive index of the lipid vesicles and increases the viscous drag in the Couette flow cell (*19*). We have previously shown for a number of cell-penetrating peptides that the use of sucrose buffers does not alter the secondary structure of membrane-bound peptides (*20*). The lipid concentration in all samples was 5 mM, and peptide was added at a peptide-to-lipid molar ratio of approximately 1:100 (corresponding to 50 μM peptide). Absorption spectra on all samples were recorded on a Cary 4000 UV−vis spectrophotometer (Varian Inc.) in a quartz cell with a 1 mm path length. Prior to measurements on the peptides, the LUV suspensions were incubated with approximately 12.5 μM retinoic acid (corresponding to 1 chromophore per 400 lipids) for at least 1 h. Retinoic acid inserts parallel to the lipid chains in a well-oriented manner and is thus an excellent spectroscopic probe of membrane lipid order, suitable for estimation of the orientation parameter S (*21*). It absorbs light in one single Gaussian-shaped absorption band centered on 352 nm, and its transition moment is oriented parallel to the molecular long axis. LD and absorption spectra of retinoic acid were recorded before addition of peptide. LD spectra were then recorded immediately after addition of peptide (the time taken to record one LD spectrum with the setting used in this study is approximately 15 min) and thereafter every 30 min for up to 2 h.

The absorption of retinoic acid overlaps to some extent the transitions from the aromatic side chains (tryptophan and tyrosine), and to more clearly show the true LD of these transitions, the contribution to LD from retinoic acid was subtracted in all LD spectra except for those shown in Figure 5. Since the LD of retinoic acid changed upon addition of peptide due to changes in microscopic ordering in the lipid vesicles (in general, a decrease was observed), the retinoic acid spectrum had to be scaled at 352 nm to subtract the correct amount. Since the magnitude of LD is concentration-dependent, the obtained peptide LD spectra were thereafter corrected for small (few micromolar) differences in peptide concentration between samples, so that each spectrum corresponds to exactly 50.0 μM.

To determine the orientation parameter in each sample, the LD from retinoic acid at 352 nm (the absorption maximum) was normalized with respect to the isotropic absorption to obtain the LD^r for the long axis transition in retinoic acid. Using $\alpha = 0°$ (insertion parallel to the membrane normal) for this transition, S was estimated using eq 2.

Peptide Transition Moments in UV−Vis Linear Dichroism. LD in the UV−vis region of the spectrum can be used to qualitatively assess the orientation of the peptide backbone through the low-energy $\pi-\pi^*$ transition which is in the plane of the peptide bond (190−210 nm) and the $n-\pi^*$ transition which is perpendicular to the plane of the peptide bond (220−230 nm). In an α-helix the $\pi-\pi^*$ transitions of neighboring peptide bonds will interact through exciton coupling and, due to the α-helix symmetry, split into two transitions, one at longer wavelengths (200−210 nm) oriented parallel to the helix axis and one at shorter wavelengths (<200 nm) oriented perpendicular to the helix axis (*22*−*24*). The latter transition cannot be resolved using our experimental setup due to the high absorptivity of the samples at such short wavelengths. The $n-\pi^*$ transitions will be

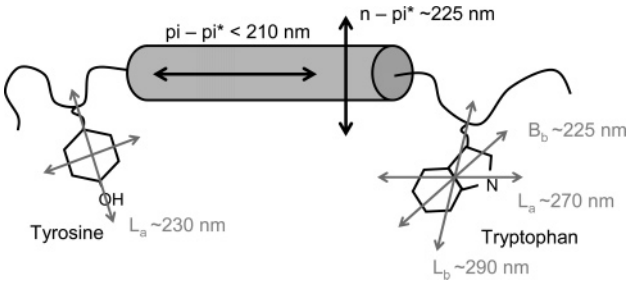

FIGURE 1: Schematic view of electronic transition moments of an α-helical oligopeptide. Peptide bond $\pi-\pi^*$ low-energy exciton transitions are polarized parallel to the α-helix, and weaker $n-\pi^*$ transitions are polarized perpendicular to the α-helix. The tryptophan side chain has three transitions localized on the indole chromophore: B_b, which is directed slightly off the pseudo symmetry axis at 225 nm, L_a with a broad absorption band in the 250−300 nm region, and L_b, which has a vibrational structure with two peaks close to 290 nm. Tyrosine has two transitions in its phenol side chain: a long-axis-polarized B_b at ~230 nm and a (mainly) short-axis-polarized L_b at 276 nm.

perpendicular to the helix axis. In addition, it is possible to use the LD from the aromatic side chains in the 220−300 nm region to obtain detailed information on their orientation relative to the membrane normal. The orientation of transition moments relative to the molecular framework of a model peptide is shown in Figure 1. Tryptophan has two overlapping electronic transitions that absorb light between 250 and 300 nm. The L_a transition is broad and largely unstructured and is the only absorbing transition above 295 nm, whereas the L_b transition has a characteristic structure with two distinct peaks near 290 nm. LD measurements on the tryptophan side chain 3-methylindole in stretched films have revealed that these transitions are oriented 85° apart in an essentially symmetric fashion around the indole pseudo symmetry long axis. L_a ($\epsilon \approx 3800$ M^{-1} cm^{-1} at 280 nm) is oriented in the direction of the nitrogen in the indole ring (−44°), and L_b ($\epsilon \approx 1900$ M^{-1} cm^{-1} at 280 nm) is oriented in the direction of the methyl substituent (+42°) which links indole to the peptide backbone (*25*). Tryptophan also has a strongly absorbing B_b transition at ~225 nm ($\epsilon \approx 36000$ M^{-1} cm^{-1}) which is oriented +11° off the pseudo symmetry long axis (in the direction toward the methyl substituent of the indole ring). Tyrosine has two perpendicular transition moments, L_a at 276 nm and L_a at 230 nm. The L_a transition is oriented parallel to the long axis of the methylphenol side chain (*26*).

Assignment of Orientation Angles and LD^r Values of Peptide Transition Moments from LD Spectra. As a first step in the interpretation of LD spectra the sign of each absorption band gives a rough picture of the insertion of the peptide. For example, in Figure 5 all spectra display positive peaks at approximately 208−210 nm, indicating that the average orientation of the α-helix is more parallel to the membrane surface than to the membrane normal. The average insertion angle of the peptide backbone was estimated from the LD^r value of this peak, but due to the competing high absorptivity at wavelengths below 210 nm from species other than the peptide existing in the sample (including lipids and buffer components), it was difficult to obtain reliable absorption spectra showing the exact absorption of the peptide bond $\pi-\pi^*$ transitions. We therefore used an approximation for the extinction coefficient of the peptide bond $\pi-\pi^*$ transition (~2000 M^{-1} cm^{-1} at 210 nm), measured for a polylysine peptide in aqueous solution (*27*), as the theoretical absorbance for each of the 22 peptide bonds in HA2(1−23) and INF7 at the wavelength where the low-energy exciton coupling displays its maximum LD. With the peptide concentration used in our LD experiments (50 μM peptide, 1 mm light path) the total absorbance in this absorption band should be approximately 0.2. It should be noted that the LD of this transition is readily measured as it is the only one giving rise to dichroic absorption at 200−210 nm.

To access more detailed information on the orientation of other peptide transition moments from LD, it is necessary to resolve overlapping transitions. Equation 2 allows for straightforward calculation of the angle relative to the membrane normal of an absorbing transition if there is no spectral overlap, but to use this equation for transitions that overlap, their relative contribution to LD must first be deduced. In this study we determined the orientation parameter *S* in eq 2 using retinoic acid (vide supra), and for the assignment of LD^r values it is convenient to divide the LD spectra by this constant to obtain LD/*S*. Using this quantity rather than LD, the determined reduced linear dichroism values (now LD^r/*S*) will be scaled to those of a perfectly aligned sample, and hence, the maximum negative LD^r/*S* is −1.5 ($\alpha = 90°$) and the maximum positive LD^r/*S* is +0.75 ($\alpha = 0°$). Since the three transitions that absorb in the "aromatic" region have different spectral profiles, it is possible to relatively accurately determine the contribution of each transition to the LD/*S* spectrum by least-squares analysis, using concentration-scaled absorption spectra for L_a(Trp), L_b(Trp), and L_b(Tyr) (here corresponding to 100 μM tryptophan and 50 μM tyrosine) as reference spectra. The fraction of each reference spectrum needed to reconstruct the measured LD/*S* spectrum corresponds directly to LD^r/*S*.

The resolved LD^r/*S* values for the transition moments in tryptophan and tyrosine that absorb in the aromatic spectral region were also used to qualitatively assign the sign and magnitude of the B_b transition in tryptophan, the L_a transition in tyrosine and the $n-\pi^*$ transitions in the peptide backbone. These three transition moments absorb light in the 220−230 nm region and have unstructured Gaussian-shaped absorption bands which overlap, thus complicating accurate analysis of the LD in this spectral region. The procedure to define the orientation of B_b(Trp) was as follows: The orientation of the plane of the indole side chain was defined by assigning directors of unit length for L_a(Trp) and L_b(Trp) in the $x-z$ plane of a Cartesian coordinate system using the information on their angles relative to the membrane normal (the *z* axis). The L_b(Trp) director was allowed to rotate around the *z* axis (in the $x-y$ plane) until the geometrically defined angle between L_a(Trp) and L_b(Trp) was 85°. The vector cross product of these two directors defines the normal vector to the indole plane. To obtain the orientation of B_b(Trp), the director for L_b(Trp) was rotated 30° around the indole plane normal, and thereafter, the angle between the B_b(Trp) director and the *z* axis could be determined. It should be emphasized that in all cases except when either L_a(Trp) or L_b(Trp) is close to any of the extreme values (0° or 90°) two unique orientations of B_b(Trp) are possible since all transition moments are uniaxially oriented around the membrane normal and LD cannot distinguish between positive and negative angles. In addition, both HA2(1−23) and INF7 contain two tryptophan residues, and since these

are indistinguishable in the LD technique, the recorded LD and all parameters derived thereof are ensemble averages of the orientations of these two residues.

Tryptophan Fluorescence Experiments. All fluorescence experiments were performed on a wavelength-corrected SPEX Fluorolog τ-3 (Jobin Yvon Horiba, France) thermostated at 25 °C. The settings for each type of experiment are detailed below.

Acrylamide Quenching. Quenching of tryptophan fluorescence by water-soluble acrylamide was used to monitor the accessibility of tryptophan to the aqueous media. A peptide or peptide−LUV solution (the peptide-to-lipid molar ratio was 1:100) containing 1 μM peptide was titrated with small aliquots of acrylamide, and the concomitant quenching of tryptophan fluorescence was measured. The samples were excited at 295 nm to avoid inner filter effects due to the absorbance of acrylamide at lower wavelengths, and emission was monitored during 30 s at 350 nm for peptide in solution and at 337 nm for peptide associated with lipid membranes. The excitation band-pass was 1 nm, and the emission band-pass was 4 nm. The ratio of the emission intensity of the unquenched sample (F_0) and the emission intensity of the quenched samples (F) was plotted against the molar concentration of quencher and analyzed according to the Stern−Volmer equation:

$$\frac{F_0}{F} = K_{SV}[Q] + 1 \qquad (4)$$

with K_{SV} the Stern−Volmer quenching constant representing the slope of a straight line fitted to the data points.

Binding Kinetics Monitored by Tryptophan Fluorescence. The time course of peptide association to lipid vesicles at pH 7.4 and 5.0 was monitored by following the change in fluorescence intensity with time after addition of 100 μM lipid vesicles to a 1 μM peptide solution. The time required for mixing and starting the experiment was 15−20 s. The excitation and emission wavelengths were set to, respectively, 280 and 335 nm, and the excitation band-pass was set to 1 nm to avoid photobleaching and light scattering. The emission band-pass was 8 nm.

Leakage of LUV-Entrapped Dyes. Peptide-induced leakage of the entrapped vesicle content was measured using the dye/quencher pair ANTS/DPX (*28*). LUVs were prepared essentially as described above, but 12.5 mM ANTS and 45 mM DPX were added to the buffer prior to the lipid film being dissolved. The LUVs were separated from nonencapsulated material by gel filtration on a Sephadex PD-10 column (Amersham Biosciences). The eluting buffer was supplemented with 100 mM sucrose to match the osmolarity of the encapsulated ANTS/DPX buffer solution. The osmolarities of the encapsulated and exterior buffers were determined using a freeze-point osmometer (Advanced 3300 Micro Osmometer, Advanced Instruments). The amount of vesicle content leakage was monitored by measuring the dequenching of ANTS that occurs upon leakage when ANTS and the quencher DPX become diluted (*28*). The excitation and emission wavelengths were set to 353 and 526 nm, respectively. The band-pass of the excitation and emission monochromator was 1 and 4 nm, respectively. The ANTS emission was monitored with time in 1 s time increments. At least 50 data points were recorded to establish the background emission level in each experiment, prior to addition of peptide. The maximum level of leakage was obtained by adding 10 μL of Triton X-100 (from a stock solution, 10% (w/v)) to the sample, which had a total volume of 1 mL. The total lipid concentration was 100 μM in all experiments. All data were corrected for background contributions by subtracting appropriate blanks. The percentage of leakage was calculated according to

$$\text{leakage (\%)} = \frac{I(t) - I_0}{I_{\text{Triton}} - I_0} \times 100 \qquad (5)$$

with $I(t)$ the emission intensity at time t, I_0 the initial intensity, and I_{Triton} the final intensity recorded after addition of Triton X-100.

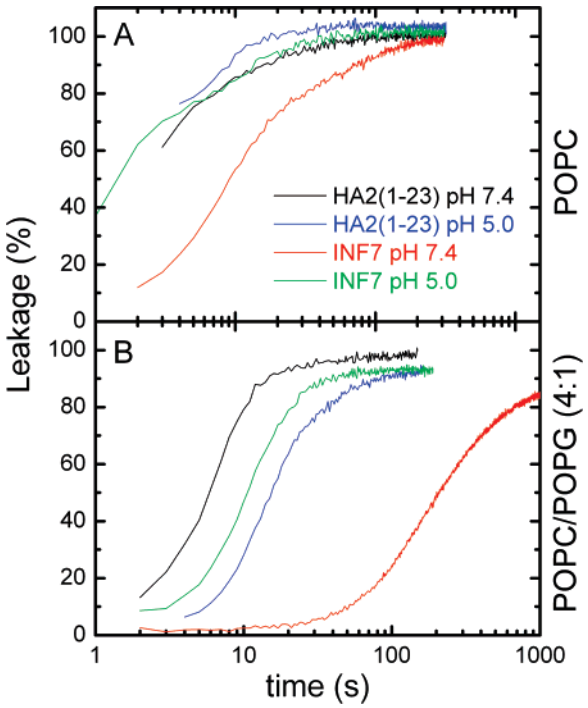

FIGURE 2: Leakage of entrapped ANTS/DPX from (A) POPC and (B) POPC/POPG (4:1) large unilamellar vesicles as a function of time (logaritimic scale) after addition of peptide. The peptide-to-lipid ratio was 1:100, and the lipid concentration was 100 μM. Each trace represents the average of three independent experiments (the spread between experiments is represented by the noise).

RESULTS

Vesicle Content Leakage. The amount of peptide-induced leakage of the encapsulated quencher pair ANTS/DPX was assessed as a measure of the membrane-disruptive capacity of HA2(1−23) and INF7 in POPC and POPC/POPG (4:1) LUVs. At a peptide-to-lipid ratio of 1:100, which is representative for all experiments in this study, these peptides are highly leakage-inducing at both physiological (pH 7.4) and endosomal (pH 5.0) conditions, as is shown in Figure 2. More than 85% leakage is observed in POPC LUVs within 2 min (Figure 2A), and HA2(1−23) caused nearly 100% leakage within as little as 10 s. Leakage induced by HA2(1−23) in POPC vesicles is insensitive to pH, which is in agreement with similar studies on leakage of encapsulated calcein from the same type of vesicles (*9*). Noticeably, in POPC/POPG (4:1) vesicles HA2(1−23)-induced leakage is

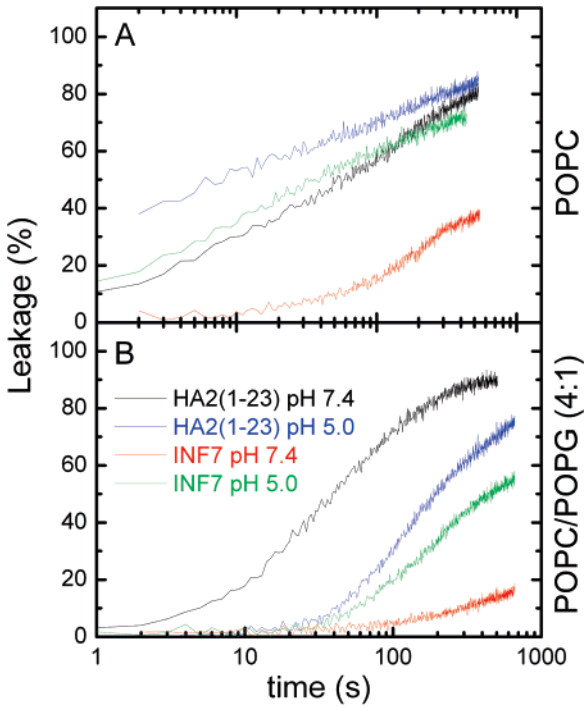

FIGURE 3: Leakage of entrapped ANTS/DPX from (A) POPC and (B) POPC/POPG (4:1) LUVs as a function of time (logarithmic scale). The peptide-to-lipid ratio was 1:1600, and the lipid concentration was 100 μM.

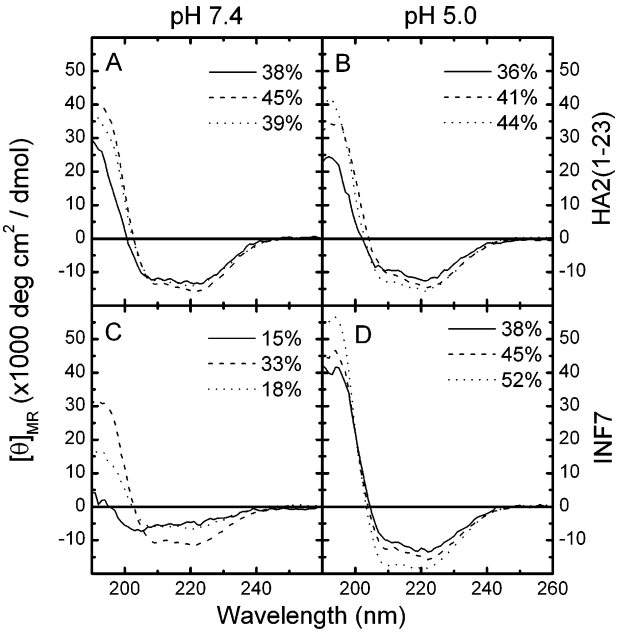

FIGURE 4: CD spectra of HA2(1−23) (A, B) and INF7 (C, D) in buffer (solid line) and in lipid vesicles composed of POPC (dashed line) or POPC/POPG (molar ratio 4:1) (dotted line) at pH 7.4 (A, C) and at pH 5.0 (B, D). The peptide-to-lipid ratio was 1:50, and the peptide concentration was 10 μM. The degree of α-helicity, calculated from the mean molar residue ellipticity at 222 nm according to Chen (*16*), is indicated in percent.

more prominent at pH 7.4 than at pH 5.0 (Figure 2B). INF7 is more potent at pH 5.0 than at pH 7.4, which confirms the hypothesis that introduction of glutamic acid residues in the N-terminal part of HA2 peptides has an effect on the pH sensitivity (*9*). The leakage half-life is approximately 1 order of magnitude longer for INF7 at pH 7.4 than at pH 5.0 in both vesicle types. To further explore the difference between these peptides in terms of induced leakage activity in LUVs, the peptide-to-lipid ratio was reduced until a significant difference in maximum leakage level was observed. Figure 3 shows time traces for leakage of ANTS/DPX from POPC and POPC/POPG (4:1) LUVs at a peptide-to-lipid molar ratio of 1:1600. As expected, leakage occurs with a much slower rate at this ratio, but still reaches relatively high levels. This clearly points out the strong membrane-destabilizing properties of HA2 fusion peptides. Also here leakage from POPC/POPG (4:1) LUVs in the presence of HA2(1−23) is faster and more efficient at pH 7.4 than at pH 5.0, which is indeed the opposite of what would be expected for this type of peptide (see Figure 3B).

Circular Dichroism. Figure 4 shows CD spectra of HA2(1−23) and INF7 at pH 7.4 and 5.0 in buffer, POPC LUVs, and POPC/POPG (4:1) LUVs. The degrees of peptide α-helicity (%), estimated as described in the Materials and Methods, are indicated in each panel. HA2(1−23) adopts an α-helical conformation (approximately 40%) under all tested experimental conditions, but there is no or little effect of lowering the pH since both the spectral shapes and the degrees of α-helicity, as determined from the mean molar ellipticities at 222 nm, are practically unchanged. The secondary structure content is in agreement with what has previously been reported for HA2(1−20) (*29*) as well as for HA2(1−20) analogues and wild-type HA2(1−23) (*14*), but while we observe HA2(1−23) to adopt secondary structure already in buffer, Lear et al. report their peptide to adopt random coil structure in the absence of lipid. Our CD observations could indicate that the peptide self-assembles in solution under the conditions used in this study. However, we never experienced any problem with insolubility or precipitation, not even at acidic pH, and saw no signs of β-sheet formation which is commonly encountered when HA2 fusion peptides aggregate.

The CD spectrum of INF7 in buffer at pH 7.4 (solid line in Figure 4C) indicates that INF7 is largely unstructured in the absence of lipid membranes. Also, INF7 shows only a modest degree of α-helicity in POPC/POPG (4:1) LUVs at pH 7.4. By contrast, at pH 5.0 INF7 is α-helical in buffer, and there is a marked increase in peptide α-helicity upon changing the pH from 7.4 to 5.0 in both types of LUVs. The CD spectrum of INF7 in buffer at pH 7.4 shows little α-helical character, nor is it a spectrum of a typical random coil. In this case it could be misleading to try to estimate α-helicity using the method of Chen et al. (*16*), and therefore, the degree of α-helicity given for this particular measurement should be treated with caution. For the purpose of this work we did not find it meaningful to further analyze the secondary structure content of INF7 in buffer at physiological pH.

Linear Dichroism. The binding geometry of HA2(1−23) and INF7 in POPC and POPC/POPG (4:1) LUVs at a peptide-to-lipid ratio of 1:100 was assessed using LD. To judge the effect of peptide binding on lipid order and to estimate the orientation factor S in eq 2, LUVs were preincubated with retinoic acid (1 chromophore per 400 lipids) as described in the Materials and Methods. Since retinoic acid orients its long axis parallel to the membrane normal, and hence perpendicular to the flow orientation axis direction (*21*), it exhibits negative LD (according to eq 1). A typical LD spectrum of retinoic acid in POPC/POPG (4:1) LUVs at pH 7.4 is shown in Figure 5 (dashed line). The

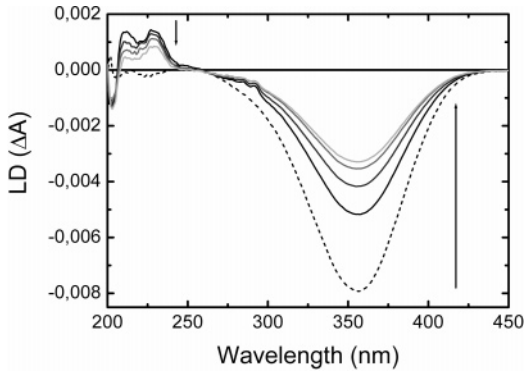

FIGURE 5: LD of HA2(1−23) in POPC/POPG (4:1) at pH 7.4 in lipid vesicles preincubated with the membrane orientation probe retinoic acid (solid line spectra). Spectra were recorded 0, 30, 60, and 90 min after addition of peptide (black to light gray). The dashed line is the LD of retinoic acid prior to addition of peptide. Arrows indicate trends of spectral change with time. The peptide-to-lipid ratio was 1:100, and the lipid vesicles contained approximately 1 retinoic acid chromophore per 400 lipids. The total lipid concentration was 5 mM.

solid lines are LD spectra of HA2(1−23) recorded 0, 30, 60, and 90 min after addition of peptide to the LUV−retinoic acid sample. These spectra show peptide-specific LD features indicative of nonrandom peptide association to the lipid membrane. Dichroic absorption can be observed from the $\pi-\pi^*$ peptide bond transitions at ∼210 nm as well as from the aromatic tryptophan and tyrosine side chains at ∼225 nm and in the 250−310 nm region. Furthermore, a marked decrease in the LD signal from retinoic acid at 352 nm can be observed immediately after addition of peptide, and this signal decreases further with time, indicating that the peptide has an effect on the membrane orientation, an observation that we shall return to.

General LD Features of HA2(1−23) and INF7. Figure 6 shows LD spectra of HA2(1−23) and INF7 in POPC and POPC/POPG (4:1) LUVs at pH 7.4 and 5.0. All spectra show a positive peak at 208−210 nm emanating from the low-energy exciton $\pi-\pi^*$ transition, whose moment is oriented parallel to the long axis of a peptide α-helix. Thus, at least the α-helical parts of the peptides are oriented more parallel to the surface than to the membrane normal, which immediately excludes stable transmembrane peptide configurations. LD will be zero for a transition that is at an angle of 54.7° (magic angle) to the membrane normal, limiting the possible average backbone orientation to the interval between 54.7° and 90° relative to the membrane normal. The magnitude of the LD from both HA2(1−23) and INF7 is, in this spectral region, small compared to that of surface-oriented penetratin peptides, which under similar conditions display approximately 5−10 times stronger LD in the $\pi-\pi^*$ absorption band (*20*, *30*). This suggests either tilted (oblique) insertion of the peptide α-helix (which would be in accord with the NMR data of Han et al. (*10*)) or general poor alignment of these peptides.

LD magnitudes are markedly weaker in all absorption bands for peptides in zwitterionic POPC LUVs (gray lines) compared to acidic (negatively charged) POPC/POPG (4:1) LUVs (black lines), indicating poor alignment in POPC membranes. With INF7 at pH 7.4 being an exception, LD can only be observed from the peptide backbone in POPC LUVs, suggesting that the aromatic side chains are completely random. We have tried to vary the peptide-to-lipid ratio in POPC LUVs to find conditions where an ordered orientation could be obtained but without success. The descriptions of the binding geometries of HA2(1−23) and INF7 will thus below be limited to what was observed in POPC/POPG (4:1) LUVs.

Most LD spectra in Figure 6 display two conspicuous positive LD peaks at ∼290 nm emanating from the L_b transition moment in tryptophan. We have previously shown that tryptophan side chains (indole chromophores) associated with LUV membranes will intrinsically adopt such an orientation as a consequence of their preferred positioning at the membrane interface (*31*).

LD of HA2(1−23) in POPC/POPG (4:1) LUVs. The LD spectra of HA2(1−23) at pH 7.4 and 5.0 in POPC/POPG (4:1) LUVs have been analyzed in detail, since these two samples display discernible LD features in the aromatic region of the spectrum and since we have here a possibility to compare our results with NMR structures for slightly shorter HA2(1−20) docked in bilayers as constructed by the group of Lukas Tamm (*10*).

The orientation factors of these two samples were estimated to be 0.026 and 0.029 at pH 7.4 and 5.0 from the LD of retinoic acid at 352 nm. Oblique insertion angles of the peptide backbones were estimated to be 60−65° relative to the membrane normal from LD of the $\pi-\pi^*$ transitions at 210 nm, using a theoretical value for the absorption at this wavelength (see the Materials and Methods). This agrees well with the oblique angle of 65° obtained using EPR on HA2-(1−20) bound to lipid vesicles equivalent to ours at pH 7.4 (*10*). However, our study provides no indication of a change in oblique insertion upon lowering the pH, whereas Han et al. (*10*) report an as much as 15° steeper insertion for HA2-(1−20) at pH 5.

The average orientation of Trp14 and Trp21 and the orientation of Tyr22 were assessed by estimating the contributions to the LD spectrum from L_a and L_b in the two tryptophan residues and L_b in tyrosine (hereafter denoted L_a-(Trp), L_b(Trp), and L_b(tyr)) using a least-squares approach described in the Materials and Methods. Figure 7 shows experimental LD/*S* curves, resolved contributions to LD from L_a(Trp), L_b(Trp), and L_b(Tyr), and reconstructed LD/*S* curves. The good agreement between the experimental and reconstructed LD/*S* curves indicates that the shape of the LD spectrum in the aromatic region is well accounted for by the above-mentioned transitions. Table 2 displays LD^r/S values and corresponding estimated angles to the membrane normal. Tyrosine is at the C-terminus of HA2(1−23) (residue 22), and given that the α-helicities in these peptides are far from 100% (see Figure 4), we reasoned that it is possible that this end of the peptide is unstructured and flexible, resulting in tyrosine not being oriented at all. We therefore also tried to resolve the LD spectra using absorption reference spectra for tryptophan only. It was, however, not possible to accurately describe the LD in the 280−300 nm region without including a contribution from L_b(Tyr). Trying to do so inevitably resulted in poor fits with strong overrepresentation of L_a(Trp) at wavelengths above 280 nm. Therefore, we conclude that all three aromatic residues in HA2(1−23) must contribute to LD and thus have a defined orientation within the membrane. This suggests that the C-terminal part

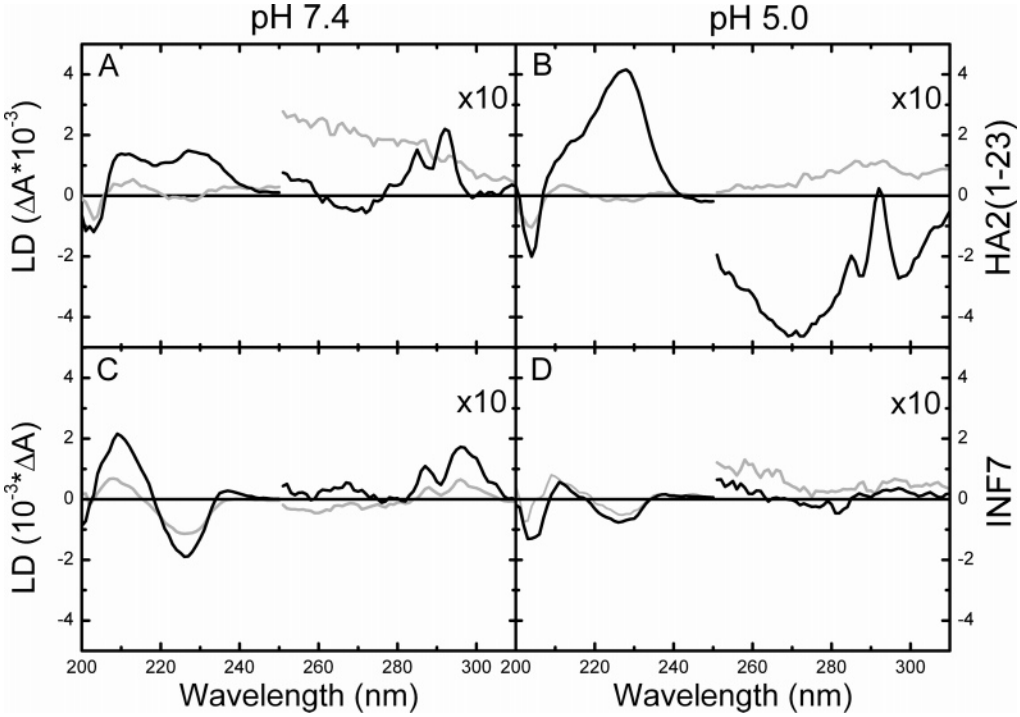

FIGURE 6: LD spectra of HA2(1−23) (A, B) and INF7 (C, D) bound to POPC lipid vesicles (gray lines) and POPC/POPG (4:1) lipid vesicles (black lines) at pH 7.4 (A, C) and pH 5.0 (B, D), recorded within 15 min after addition of 50 μM peptide to a lipid vesicle suspension with a total lipid concentration of 5 mM. The spectra have been magnified 10 times in the 250−310 nm region to facilitate visualization of spectral features from the aromatic amino acids in the peptides. All spectra were recorded in the presence of membrane orientation probe retinoic acid added prior to peptide addition at a chromophore-to-lipid ratio of 1:400. For clarity, the spectral contribution from this chromophore (see Figure 5) has been subtracted.

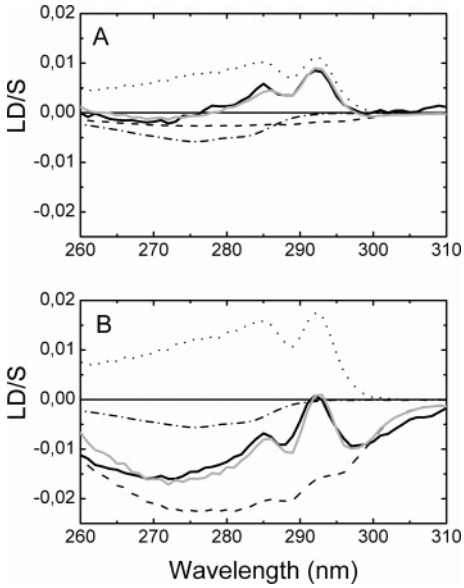

FIGURE 7: Resolved LD spectra in the aromatic region of HA2-(1−23) in POPC/POPG (4:1) lipid vesicles at pH 7.4 (A) and pH 5.0 (B). Measured (solid gray lines) and reconstructed (solid black lines) LD spectra and also LD spectral components of L_a(Trp), L_b-(Trp), and L_b(Tyr) (dashed, dotted, and dashed−dotted lines, respectively) are shown.

Table 2: LD^r Values and Concluded Angles (α) of Peptide-Specific Transition Moment Angles Relative to the Membrane Normal for HA2(1−23) in POPC/POPG (4:1) Large Unilamellar Vesicles at pH 7.4 and 5.0[a]

		pH 7.4		pH 5.0	
chromophore	transition	LD^r/S	α	LD^r/S	α
Trp	L_a	**−0.07**[b]	**53**	**−0.58**	**40**
	L_b	**+0.47**	**69**	**+0.72**	**84**
	B_b	*∼0*[c]	*∼55*	*∼+0.25*	*60−65*
Tyr	L_b	**−0.80**	**34**	**−0.77**	**35**
	L_a	*∼+0.70*	*80−90*	*∼+0.70*	*80−90*
peptide bond	$\pi-\pi^*$	*+0.27*[d]	62	+0.22	61

[a] LD^r for each sample, normalized with respect to the orientation factor determined by the retinoic acid probe. The maximum possible $LD^r/S = +0.75$ ($\alpha = 90°$), and the maximum negative $LD^r/S = -1.5$ ($\alpha = 0°$). [b] Parameters in bold were resolved by least-squares projection of LD spectra, normalized with respect to the order parameter *S*, onto reference absorbance spectra in the aromatic region (255−310 nm) as shown in Figure 7. See the Materials and Methods. [c] Parameters in italics were estimated by applying geometric constraints for planar chromophores of tryptophan and tyrosine side chains. [d] The LD^r/S values defining the oblique insertion angles of the peptide backbone were estimated from the experimental LD and extinction coefficient for the $\pi-\pi^*$ transition at 210 nm as described in the text (Results).

of HA2(1−23) adopts an at least partly ordered orientation in POPC/POPG (4:1) LUVs at both pH 7.4 and pH 5.0.

From the LD^r/S values and insertion angles for L_a(Trp) and L_b(Trp) theoretically possible limiting orientations for B_b(Trp) were calculated (see the Materials and Methods). At pH 7.4 the B_b(Trp) transition moment was estimated to have an average orientation that is either very close to the magic angle or close to 90°; that is, its LD should be either zero or close to the maximum possible. The magnitude of the LD at ∼225 nm is not large enough to allow the orientation of B_b(Trp) to be 90°; therefore, we accept the near magic angle alternative as the true one (see Table 2). At pH 5.0, B_b(Trp) was estimated to be 60−65° from the membrane normal.

The L_b(Tyr) transition moment is oriented 35° from the membrane normal at pH 7.4 as well as at pH 5.0, indicating that Tyr22 does not significantly change its binding geometry

in the lipid membrane when the pH is lowered. The L_b(Tyr) and L_a(Tyr) transition moments are at right angles to each other in the plane of the tyrosine side chain, and this geometric constraint prohibits both simultaneously displaying negative LD. Therefore, L_a(Tyr) must also contribute to the positive LD signal in the 220−230 nm region. We explain the LD in the 220−230 nm as follows: The n−π* transitions in the peptide backbone give rise to a weak negative LD contribution at both pH 7.4 and pH 5.0. According to our estimate of the insertion angles of the peptide backbone from the $\pi-\pi$* transition, the peptide backbone does not change its orientation to any significant extent upon lowering the pH, and thus, also the n−π* transition should display an LD of invariant magnitude. The L_a(Tyr) transition contributes to a positive LD at both pH 7.4 and pH 5.0, and due to the fact that Tyr22 does not change its conformation, this contribution is of constant magnitude. We therefore assign the observed increase in LD (see black lines in Figure 6A,B) at ∼225 nm upon changing the pH from 7.4 to 5.0 to a change in orientation for B_b(Trp) from approximately magic angle insertion (∼55°) at pH 7.4 to 60−65° at pH 5.0. This change corresponds to an increase in LD^r/S of +0.25, which when recalculated into LD units corresponds almost exactly to the observed increase in the LD signal at 225 nm.

LD of INF7 in POPC/POPG (4:1) LUVs. At pH 7.4 INF7 (Figure 6C, black line) displays significantly larger LD in the $\pi-\pi$* absorption band at 210 nm compared to HA2(1−23). The average insertion angle of the peptide backbone relative to the membrane normal was estimated to be ∼70°, indicating that INF7 inserts more parallel to the membrane surface, possibly related to a difficulty for this peptide to insert the negatively charged Glu4 and Glu 7 residues into the hydrocarbon core. In the aromatic region there is a clear positive contribution to LD from L_b(Trp), whereas the LD is essentially zero between 260 and 280 nm, indicating that neither L_a(Trp) nor L_b(Tyr) gives rise to net LD in this region. The negative contribution to LD at 225 nm is in part due to the relatively weak n−π* transitions, oriented perpendicular to the peptide α-helix, but the magnitude of this peak suggest that also the aromatic side chains contribute in this region; presumably this peak is enlarged due to a negative LD from B_b(trp).

At pH 5.0 INF7 displays no discernible LD in the 250−310 nm region, and the magnitude of the $\pi-\pi$* transition at 210 nm is reduced approximately 4-fold compared to that at pH 7.4 (Figure 6C, black line). It is thus clear that the interaction between INF7 and the POPC/POPG (4:1) LUV membrane is dramatically different from the interactions observed for HA2(1−23). The lack of orientation for aromatic side chains indicates multiple binding modes, and the weak LD at 210 nm indicates that at least some fraction of the peptides penetrate deeper into the membrane, resulting in the average insertion of the peptide backbone being close to the magic angle (54.7° from the membrane normal).

Time-Dependent LD of Lipid Order Probe Retinoic Acid. The evolution of LD from retinoic acid with time was followed by recording LD spectra every 30 min after peptide addition, and Figure 8 shows the retinoic acid LD at the wavelength of maximum absorption normalized with respect to the initial signal obtained before addition of peptide. The retinoic acid LD decreases markedly immediately after addition of peptide to POPC LUVs (Figure 8A). The POPC

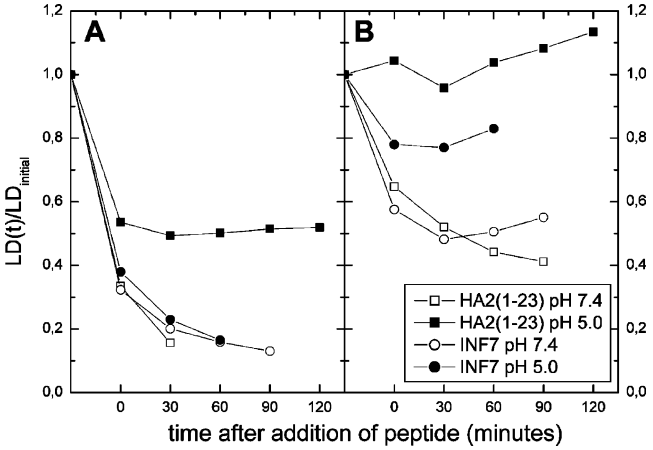

FIGURE 8: Relative LD of membrane probe retinoic acid, LD(*t*)/$LD_{initial}$, showing the change in membrane orientation of shear-deformed LUVs with time upon addition of peptide (added at time 0). Each trace starts at $LD(t)/LD_{initial} = 1$, which represents the initial retinoic acid LD recorded on the LUV sample prior to addition of peptide. Data are shown for HA2(1−23) (squares) and INF7 (circles) at pH 7.4 (open symbols) and at pH 5.0 (filled symbols). The LUV lipid composition was POPC (A) or POPC/POPG (4:1) (B).

membranes are least perturbed by HA2(1−23) at pH 5.0. In POPC/POPG (4:1) LUVs the retinoic acid LD is significantly less reduced than in POPC LUVs, which is in agreement with the overall better peptide orientations observed in Figure 6. The change in retinoic acid LD in POPC/POPG (4:1) LUVs is pH dependent, and at pH 5.0, addition of HA2(1−23) even results in a minor increase in retinoic acid LD with time.

A change in retinoic acid LD is a consequence of changed overall orientation in the sample and may be caused by a change in lipid chain order, in vesicle deformability, or in vesicle alignment. The trivial cause that the decreased LD is due to a decreased number of vesicles in the light path due to, for example, vesicle lysis or precipitation must first be excluded. From experiments using the detergent Triton-X we know that complete vesicle lysis results in a total loss of LD (results not shown). Absorption measurements indicate that no precipitation occurred since the peptide concentrations in the samples (measured after the LD experiments were completed) were always as expected. As a control, dynamic light scattering was used to establish that the vesicle size distribution remained constant. Addition of peptide to the LUVs at the peptide-to-lipid ratios and total concentrations identical to those used in the linear dichroism as well as all fluorescence spectroscopy experiments had no detectable effect on the count rate (scattering intensity) or shape of the autocorrelation functions. Estimated hydrodynamic radii and polydispersity indexes calculated using second-order cumulant analysis remained constant even after more than 2 h of incubation (data not shown). In addition, while fluorescence experiments were being performed, static light scattering intensity from LUV samples was routinely monitored with time after addition of peptide using a SPEX Fluorolog τ-3 fluorimeter with excitation and emission monochromators set to 600 nm. The scattered intensity remained constant, indicating that vesicle aggregation did not occur (*32*). Taken together the above controls indicate that the LUVs maintained integrity during the experiments, and we therefore

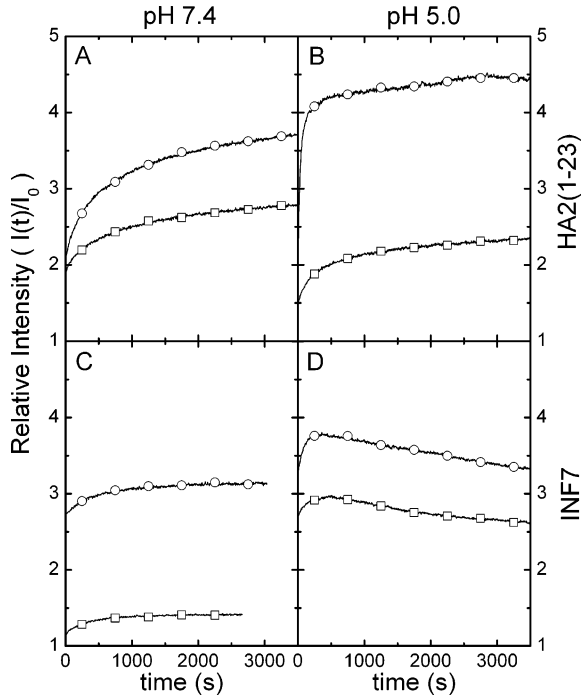

FIGURE 9: Kinetics of peptide binding to lipid vesicles monitored as the relative change in intensity of peptide tryptophan fluorescence, $I(t)/I_0$. $I(t)$ is the emission intensity at time t after addition of lipid vesicles (POPC (circles) and POPC/POPG (4:1) (squares)) to samples containing HA2(1−23) (A, B) or INF7 (C, D) at pH 7.4 (A, C) or pH 5.0 (B, D). I_0 is the emission intensity of the same sample prior to addition of peptide. The peptide-to-lipid ratio was 1:100 and the lipid concentration 100 μM.

exclude both complete lysis and vesicle aggregation as causes of the observed loss in retinoic acid LD.

Peptide−Lipid Interaction Kinetics Probed by Tryptophan Fluorescence. Binding of peptide to LUVs was assessed by monitoring the tryptophan emission intensity with time as well as by recording emission spectra. Transfer of peptide from buffer to the LUV membrane resulted in blue-shifted tryptophan emission and a concomitant intensity increase. Figure 9 shows time traces of the tryptophan fluorescence from peptide samples recorded after addition of POPC or POPC/POPG (4:1) LUVs. The intensity is expressed in relative units with respect to the emission intensity of the peptide in water. None of these traces can be fitted with a monoexponential function, which suggests that the binding of HA2(1−23) and INF7 to both POPC and POPC/POPG (4:1) lipid membranes is a multistep process. The shapes of the curves indicate a fast first step, in which the peptides presumably associate with the lipid bilayer. It should be noted that the leakage of entrapped content reported in Figure 2 is completed during this phase. Thereafter follows one or several slower steps which may be related to peptide rearrangement in the membrane. The emission intensity increases on average ∼3-fold, which must be regarded as extreme compared to measures obtained for membrane-bound penetratin peptides (∼1.5-fold increase) (*20*). This effect is more pronounced in POPC LUVs than in POPC/POPG (4:1) LUVs. Binding of INF7 to POPC/POPG (4:1) LUVs at pH 7.4 (Figure 9C) is associated with a noticeably smaller increase in intensity than that of all other peptide−lipid vesicle combinations, but it is, as indicated above, readily comparable to what we have previously observed for the surface-bound CPP penetratin (*20*). At pH 5.0 (Figure 9D), INF7 first displays a fast initial binding step, resulting in an expected increase in emission intensity, but thereafter, a slow but steady decrease follows, implying that the tryptophan residues slowly become more accessible to water again.

The emission maximum wavelength of tryptophan can give a rough estimate of how deep this residue penetrates into the membrane (*33*). For a peptide that associates in the membrane headgroup region the emission maximum is centered at 337−340 nm (*20*). We observe emission maximum wavelengths typically below 333 nm for membrane-bound HA2(1−23) and INF7 in agreement with previous reports for HA2(1−20) (*29*, *34*). This indicates some penetration into the hydrocarbon core for the tryptophan residues, but does not correspond to a completely apolar environment where the emission maximum can approach 320 nm (*26*). INF7 at pH 7.4 in POPC/POPG (4:1) LUVs is an exception and exhibits a tryptophan emission maximum at 341 nm, again indicating that its tryptophan residues are in an environment similar to that of tryptophan residues of surface-bound peptides.

Tryptophan Emission Quenching by Acrylamide. Acrylamide quenching experiments were performed to further assess the shielding of tryptophan residues from water. Figure 10A shows Stern−Volmer plots for the quenching of tryptophans in HA2(1−23) at pH 7.4 in buffer, POPC vesicles, and POPC/POPG (4:1) vesicles. The quenching of free tryptophan in buffer is shown for comparison. Similar linear Stern−Volmer plots were obtained in all experiments, indicative of a relatively homogeneous longitudinal distribution of the tryptophan residues (*26*), therefore suggesting that Trp14 and Trp21 are equally susceptible to quenching and thus reside in similarly protected environments. Figure 10B shows Stern−Volmer quenching constants, K_{SV}, for HA2(1−23) or INF7 at pH 7.4 or 5.0 in buffer, POPC LUVs, or POPC/POPG (4:1) LUVs as well as for tryptophan in buffer (this K_{SV} value was independent of pH). Figure 10B reveals that tryptophan residues in both HA2(1−23) and INF7 are significantly shielded from water already in buffer, which in turn strongly indicates that these peptides assemble in solution. This is further supported by our observations that the maximum wavelengths of tryptophan emission for the peptides in buffer were significantly less than the ∼352 nm measured for tryptophan alone (below 340 nm for HA2(1−23) and below 345 nm for INF7 at pH 5.0). INF7 in buffer at pH 7.4 is an exception: Displaying maximum emission at 348 nm, this peptide is probably not significantly aggregated in solution, which is also manifested in the larger K_{SV}. From helical wheels constructed for the peptide sequence it is evident that the two tryptophan residues in both HA2(1−23) and INF7 should be positioned at the edge of the nonpolar face if the entire peptide is α-helical, and it is thus envisaged that the tryptophan residues will be significantly shielded from water if the peptides associate to avoid displaying their hydrophobic side to the aqueous surrounding. Lowering the pH from 7.4 to 5.0 lowers the K_{SV} for the free peptides even further, which is to be expected since the water solubility of the peptides should be significantly reduced upon protonation of the glutamic acid side chains. When bound to liposomes, HA2(1−23) displays $K_{SV} \approx 2$, and there is no or little effect of varying the LUV type or pH. The values reported here are somewhat lower

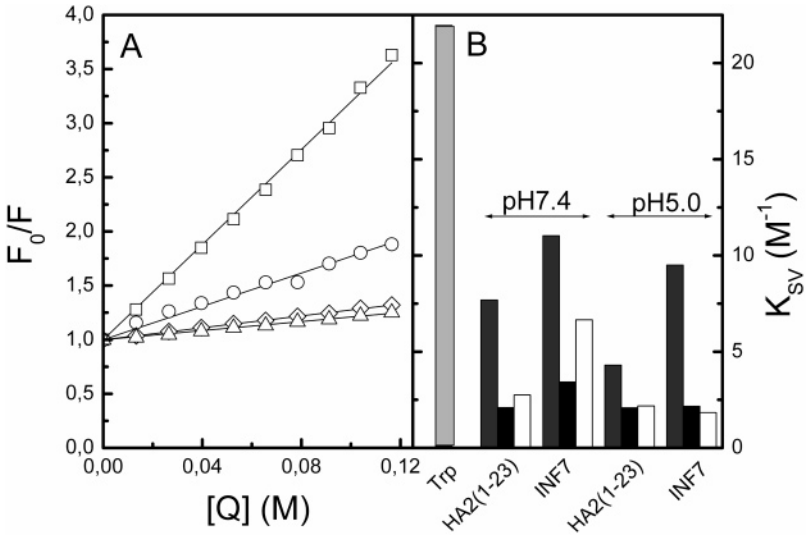

FIGURE 10: Stern−Volmer plots (A) and Stern−Volmer quenching constants (B) showing the degree of quenching of tryptophan fluorescence by the presence of (water-soluble) acrylamide. (A) The degree of quenching of the tryptophan residues in HA2(1−23) in different environments (buffer (circles), POPC vesicles (triangles), and POPC/POPG (20/80) vesicles (rhombuses)) is compared to that of free tryptophan in buffer (squares). (B) Stern−Volmer quenching constants. The light gray column corresponds to Trp in buffer. The other columns show HA2-(1−23) and INF7 at pH 7.4 and 5.0 in buffer (dark gray), in POPC lipid vesicles (black), and in POPC/POPG (4:1) vesicles (white).

compared to earlier observations for HA2(1−25) in DMPC vesicles (*34*). The K_{SV} values for INF7 bound to LUVs are similar to that of HA2(1−23) at pH 5.0, except that for INF7 in POPC/POPG (4:1) LUVs at pH 7.4, which is significantly higher.

DISCUSSION

This work comprises a linear dichroism study of HA2 fusion peptides in zwitterionic and acidic lipid membranes of large unilamellar vesicles (100 nm), where we assess the orientation of the peptide backbone and also gain detailed information on the binding geometry from the positioning of the aromatic tryptophan and tyrosine side chains. In addition, we explore the effects of peptides on the vesicle lipid bilayer, properties that we will relate to the leakage-inducing capacity. As mentioned in the introduction, HA2 fusion peptides have been extensively studied in the past, foremost with the aim of understanding the mechanisms by which the influenza virus infects cells. Despite this, we are here first to report on the orientation of an unlabeled HA2 peptide when bound to a lipid vesicle model membrane and to point out a marked difference in the mode of interaction of HA2 peptides with zwitterionic (POPC) and slightly acidic (POPC/POPG (4:1)) lipid membranes. Finally, we find that HA2 peptides interact with lipid membranes in a time-dependent fashion, the origin of which will be discussed.

Leakage-Inducing Capacity. We set out to explore the relation between structure and membrane-perturbing properties of HA2 fusion peptides with a perspective on future implementation of such peptides in existing strategies for peptide-mediated drug delivery to enhance endosomal escape. Within this scope, selective membrane destabilization at endosomal pH is a qualifying property of the delivery system. We show in Figures 2 and 3 that both HA2(1−23) and INF7 are indeed highly potent in causing leakage of small organic molecules at moderately to extremely low peptide-to-lipid ratios. However, HA2(1−23) is not significantly discriminatory to pH in terms of induced leakage. This has been observed before (*9*) and is in fact not so surprising since it is likely that the HA2 fusion peptide itself is buried within the hemagglutinin protein at pH 7.4 and only exposed at the membrane surface at pH 5.0 (*35*). In addition, even though Glu11 and Asp19 are highly conserved in influenza A virus strains, studies on point-mutated HA proteins expressed on the surface of CV-1 cells indicate that neutralization of these residues may not even be necessary for targeting lipid bilayers and initiating fusion (*36*). Thus, in nature, built-in pH sensitivity in the fusion peptide sequence may not be essential.

By contrast, INF7 is pH-sensitive in terms of induced leakage, reaching levels similar to those of the wild-type HA2(1−23) at pH 5.0 but significantly reduced levels at pH 7.4. At a peptide-to-lipid ratio of 1:100 this primarily manifests in slower establishment of maximum leakage levels, but since the turnover time for lipids in the plasma membrane is relatively short in mammalian cells with normal endocytotic activity (for example, 50% of the surface area of fibroblasts is interiorized in 1 h (*37*)), this type of kinetic discrimination may be sufficient to minimize leakage at the surface of the plasma membrane relative to leakage obtained in the endosome. Despite the fact that both HA2(1−23) and INF7 induce nearly 100% leakage, we see no signs that LUVs may burst in the presence of peptide, which may indeed be a limitation when it comes to release of larger endosome-entrapped cargo such as DNA or full-length proteins.

Secondary Structure and pH Sensitivity. A relationship between the secondary (α-helical) structure and fusion ability of HA2 peptides was earlier proposed: The basis of this mechanism may be steric clash or electrostatic repulsion between glutamic acid residue side chains in the folded state, preventing stable α-helix formation at physiological pH (*9*, *14*). From CD we confirm that the Glu4 and Glu7 introduced in the mutated INF7 indeed prevent efficient α-helix formation in buffer at pH 7.4, but since addition of lipid immediately induces α-helicity already at physiological pH, it seems less likely that electrostatic repulsion between the glutamic acid residues could be the only origin of pH

sensitivity of the INF7 peptide, at least not in zwitterionic membranes where the negatively charged side chains could interact with positively charged choline headgroups and thus screen their charge. In POPC/POPG (4:1), where pH sensitivity is more pronounced, the situation is somewhat different. The α-helical content increases from 18% to 52% when the pH is lowered from 7.4 to 5.0. Under similar conditions HA2(1−23) is 39% and 44% α-helical. Thus, Glu4 and Glu7 are concluded to repel each other and prevent helix formation of the N-terminal.

Binding Geometry of HA2(1−23) in POPC/POPG (4:1) LUVs. HA2(1−23) in POPC/POPG (4:1) exhibits a remarkably high degree of orientation, which allowed us to resolve orientation details of its aromatic residues (see Table 2). The fact that the insertion angle of the L_b(Trp) transition at pH 5.0 conditions could be estimated to be 84°, despite the fact that it represents an average of the two tryptophans in HA2-(1−23), suggests that both these residues have a strong propensity to orient themselves with this transition close to parallel to the membrane surface. Furthermore, this suggests that at least these residues, and very likely the entire peptide, are well-aligned in the lipid membrane since any heterogeneity among the peptides would result in cancellation of the effects and decreased average LD. The observed oblique insertion angles (Table 2) of the peptide backbone are in agreement with previous reports and support the possibility that HA2(1−23) could be inserted in a crescent-shaped "boomerang" fashion (*10*). HA2(1−23) undergoes some conformational change upon reduction of pH (see Figure 6 and Table 2), but as concluded in the Results this has in our hands no visible effect on the oblique insertion angle of the peptide backbone. In addition, our LD results indicate that the orientation of Tyr22 at the C-terminal end of HA2(1−23) is virtually unaffected by pH. Thus, it is reasonable to propose that also the neighboring Trp21 maintains its orientation when the pH is changed. Tryptophans and tyrosines have a strong bias to reside in the membrane interfacial region (*38*), and the LD of the tryptophan side chains has the same features as that observed for tryptophan model compounds with interfacial positions such as indole and 3-methylindole when bound to LUVs (positive L_b and B_b, negative L_a (*31*)). Therefore, we suggest that interfacial pH-independent interactions of Trp21 and Tyr22 drive the positioning of the HA2(1−23) C-terminal, serving to anchor this part of the peptide at the membrane interface. This indicates that the flexibility of HA2 peptide C-termini observed in NMR for both wild-type and mutated versions of HA2(1−20) (*10*, *13*) is reduced if the peptide is elongated so that these two aromatic side chains are included. This result may have implications for the understanding of how the HA2 fusion peptide domain functions when part of the hemagglutinin protein.

Taken together, LD data suggest that the conformational change in the membrane-bound HA2(1−23), observed upon lowering the pH, does not involve any major repositioning of the peptide backbone, nor is the C-terminus significantly affected. One may therefore envisage that a local conformational change occurs in the hinge region (*10*) which encompasses Trp14 and is flanked by pH-sensitive Glu11 and Glu15. According to LD data, this conformational change involves repositioning of Trp14, resulting in the indole chromophore long axis being rotated toward an insertion more parallel to the membrane surface at pH 5.0. This rotation could be consistent with the possibility that Trp14 "swings out" from the hydrophobic pocket in the hinge region and adopts an orientation similar to that in the NMR model of HA2 analogue E5 proposed by Hsu et al. (*13*).

Binding of INF7 to POPC/POPG (4:1) LUVs. We confirm that INF7 displays some promising pH sensitivity regarding the capacity to induce leakage, especially in POPC/POPG (4:1) LUVs (Figures 2 and 3). This manifests foremost in reduced leakage activity at pH 7.4 compared to that of HA2-(1−23). However, under these experimental conditions INF7 also displays the smallest increase in tryptophan fluorescence intensity upon membrane binding, the lowest Stern−Volmer quenching constant (K_{SV}), and the highest emission maximum wavelength observed for any of the peptide−lipid−pH combinations tested in this study. In addition, INF7 is only moderately α-helical (18%). These observations imply that the pH sensitivity of INF7 could primarily be due to poor membrane association at pH 7.4, a property not ideal from a drug-delivery perspective since it could potentially reduce the uptake efficiency of the vector. Few attempts have been made to characterize the binding affinity of HA2 peptides, presumably since their highly hydrophobic character strongly favors complete membrane association, but also because their hydrophobicity complicates the analysis of binding data as noted by Vaccaro et al. (*39*). We did try to construct binding isotherms from tryptophan fluorescence spectra recorded during titration of the peptide to an LUV solution. However, this procedure did not yield any informative results due to peptide aggregation in solution and likely also in the membrane (vide infra), obstructing the necessary definition of "free" and "bound" states (*40*). According to estimates by Lear et al. (*29*), HA2(1−20) associates completely with small unilamellar vesicles composed of POPC at peptide-to-lipid ratios above 1:75. INF7 may be expected to display lower affinity since Glu4 and Glu7 increase water solubility and decrease hydrophobicity. Using the Wimley and White intrinsic whole-residue hydrophobicity scale (*41*), the theoretical free energy of partitioning the INF7 peptide from water to the interface of a POPC membrane was calculated to be −4.3 kcal/mol taking into account the acetylated N-terminus and amidated C-terminus as well as the observed peptide α-helical content (*42*). This corresponds to, at room temperature, an equilibrium partition constant of $\sim 10^3$, indicating that the equilibrium is strongly shifted toward membrane association. Naturally, the membrane binding affinity could be expected to be somewhat lower in the presence of POPC/POPG (4:1) LUVs due to the fact that 20% of the lipids in these vesicles carry a net negative charge. However, returning to our own results, we reemphasize that the tryptophan fluorescence properties of INF7 indeed resemble those of the CPP penetratin which interacts strongly with lipid membranes by interactions in the headgroup region (*20*). In addition, INF7 displays the, for this study, largest LD^r in the $\pi-\pi^*$ absorption band, which in fact disputes poor membrane association. The LD at 210 nm could be exploited to derive a lower limit of the bound fraction of INF7. Under the assumption that all bound INF7 peptides bind with their entire backbone perfectly parallel to the lipid plane, the LD observed in Figure 6C would correspond to at least 55% of the peptides being membrane bound. Perfect orientation is not likely achieved because of

the dynamic properties of the membrane and due to the fact that far from 100% of the peptide is α-helical. Therefore, we can safely conclude that significantly more than 55% has to be bound. Thus, even though direct experimental evidence in terms of binding constants cannot be provided, the above argumentation taken as a whole suggests that the major fraction of added INF7 peptide associates with the POPC/POPG (4:1) LUV membrane at a peptide-to-lipid ratio of 1:100. Therefore, the reduced leakage capacity at pH 7.4 cannot be explained solely by poor membrane association even though we cannot exclude that this could have some minor effects.

Possible Structural Origins of INF7 pH Sensitivity. Leaving the discussion of whether poor membrane binding may to some extent influence the pH sensitivity of INF7, we shall now focus attention on structural and physicochemical features differentiating the membrane interactions of INF7 at pH 7.4 and 5.0. CD indicates that, upon binding to POPC/POPG (4:1) LUVs, INF7 cannot adopt much α-helical structure (18%), whereas HA2(1−23) under similar conditions is 39% α-helical. With the only difference between these two peptides being the introduction of glutamic acid residues in INF7 at positions 4 and 7, it is reasonable to suggest that the N-terminal part of INF7 is hindered from adopting α-helical structure in the membrane milieu, likely due to the fact that these negatively charged residues repel each other. As mentioned above, several tryptophan fluorescence parameters speak in favor of Trp14 and Trp21 in INF7 residing in the headgroup region. In addition, the LD^r magnitude in the $\pi-\pi^*$ absorption band corresponds to an oblique angle of ∼70°, despite the fact that only a small portion of the peptide takes part in the α-helical structure where $\pi-\pi^*$ transitions are expected to be stronger due to exciton coupling. This points to a more surface-oriented binding of INF7 compared to HA2(1−23). The free energy cost of partitioning one charged glutamic acid residue from water into octanol amounts to ∼3.6 kcal/mol (*43*), indicating that it should be virtually impossible for the N-terminal segment of INF7 to be inserted into the hydrocarbon core. By contrast, the free energy cost for partitioning of a protonated glutamic acid residue is only ∼0.1 kcal/mol, indicating that at low pH insertion of this segment may occur. Recent estimates of pK_a values of each individual negatively charged amino acid in HA2(1−25) and the glutamic acid-enriched analogues E5(3,7) and E5(4,8), determined in negatively charged SDS micelles, indicate that all glutamic acid residues and Asp19 have pK_a values at least 1 log unit above the standard value for glutamic acid residues (pK_a = 4.3) (*8*). By contrast, in zwitterionic DPC micelles the pK_a of Glu4 in a 20-residue E5 peptide was estimated to be ∼4.2, whereas Glu8, Glu11, and Glu15 had $pK_a \approx 5.4$(*44*). These observations suggest that at pH 5.0 70−80% of the negative charge on the glutamic acid residues can be expected to be neutralized. Glutamic acids in the very N-terminal (Glu4) may be an exception, but it is possible that negative lipids in the headgroup region promote protonation of such residues and thus insertion into the hydrocarbon core. The driving force could be to minimize electrostatic repulsions between the lipid headgroups and peptide.

Two different NMR models have been proposed for the glutamic acid-enriched HA2 peptide E5 (GLFEAIAIFIEGGWEGLIEG), both acquired in DPC micelles. Hsu et al. (*13*) propose that the pH-sensitive mechanism of E5 is essentially the same as the one proposed by Han et al. (*10*) and point out the importance of the hinge region around Trp 14. Their model assumes that Glu4 and Glu8 have a negligible effect on the insertion of the N-terminus, probably because both these residues are on the hydrophilic phase of the helix and can reside in the headgroup region even if the peptide backbone is inserted. By contrast Dubovskii et al. (*44*) suggest no pronounced hinge motif but suggest that the E5 peptide acts as an amphipathic helix and that protonation of the foremost Glu11 promotes relocation of the peptide into the hydrocarbon core at low pH. This is also concomitant with stabilization of the α-helical structure. Even though the INF7 primary structure is not identical to that of E5, they share sufficient analogy to be compared: Both CD and LD data for INF7 indicate that this peptide behaves differently from HA2(1−23). The marked increase in α-helix content, the surface-oriented structure at pH 7.4 indicated in LD, and the transfer of tryptophan residues from the headgroup region into a more hydrophobic environment upon lowering the pH (indicated from tryptophan fluorescence measurements) speak in favor of the pH-dependent membrane interactions of INF7 more resembling Dubovskii's model than Hsu's. Unfortunately, it is obvious from LD data (Figure 6D) that INF7 is no longer well aligned at pH 5, suggesting that in a lipid bilayer as opposed to a micellar environment several orientations become accessible, resulting in averaging that inevitably reduces LD. This cannot be explained by overall poor alignment of the sample but must result from different backbone conformations (see Figure 8B). A possible cause of multiple peptide orientations is self-assembly within the membrane, which has been reported to occur (*8*, *45*, *46*). Peptide self-assembly could be driven by interactions between Glu4 and Glu7 on neighboring INF7 peptides.

Long-Term Changes in Peptide−Membrane Interactions. The membrane-destabilizing effect of both HA2(1−23) and INF7 manifests in the observation that encapsulated small dyes can equilibrate across LUV membranes within minutes after peptide addition. Nevertheless, even after leakage has reached 100%, we can observe a slow monotonous increase in peptide tryptophan emission intensity (Figure 9) and a decrease in LD of membrane orientation probe retinoic acid (Figure 8), suggesting that the peptide−lipid interactions do not reach an equilibrium state with the completion of leakage. The decrease in retinoic acid LD indicates that the upper part of the hydrocarbon core slowly becomes more and more disordered due to interactions with HA2 peptides, a process that is seemingly accompanied by more efficient shielding of peptide tryptophans from water. In POPC LUVs this behavior is coincident with poor peptide alignment, manifested in weak peptide bond LD and indiscernible orientation of peptide aromatic side chains (Figure 6). Why such poor orientation is obtained in POPC LUVs whereas incorporation of a rather small portion of negatively charged lipid headgroups in the POPC/POPG (4:1) LUVs gives much better order is not easily understood. It seems as if some sort of collapse occurs in the headgroup region of POPC membranes possibly due to interactions between lipid cholines and peptide glutamic acids. Note that Han et al. chose to construct their EPR model of HA2(1−20) in DOPC/DOPG (4:1) LUVs even though their NMR model was obtained in zwitterionic DPC micelles (*10*).

The observations of poor peptide orientations that are gradually worsened with time could indicate peptide self-assembly within the membrane, which has been reported to occur (*8*, *45*, *46*). The lack of observable aromatic residue LD suggests that such assemblies are of disordered nature. Since the positioning of the peptide backbone is more restricted by the membrane than the positioning of individual side chains, there is still an observable bias toward a preferentially more parallel than perpendicular insertion. Peptide assembly could potentially help in shielding negatively charged residues, thus allowing the peptide backbone to penetrate deeper into the membrane, the result being smaller LD magnitudes as well as decreased lipid chain order. A correlation between reduced lipid chain order and oblique insertion was found from molecular dynamics simulations of HA2 peptides in POPC membranes (*39*). As mentioned in the Results, we performed control experiments to verify that the LUVs were indeed intact, despite their extensive leakiness and the observed reductions in retinoic acid LD. To our surprise we found no indications that the LUVs would actually burst or that other types of peptide−lipid aggregates would form.

Correlation between Leakage Levels and Orientation. A general conclusion from this work is that leakage is more prominent in zwitterionic POPC LUVs than in slightly acidic POPC/POPG (4:1) LUVs. Interestingly, as probed by retinoic acid, we can also see some correlation between leakage efficiency and the lipid membrane disorder observed immediately after addition of peptide to LUVs. This correlation may in fact also explain the somewhat surprising observation that HA2(1−23) is even more potent as a leakage-inducing peptide at pH 7.4 than at pH 5.0 in POPC/POPG (4:1) LUVs since in Figure 8 we show that HA2(1−23) does not decrease the lipid chain order at all at pH 5.0, whereas a significant effect is observed at pH 5.0. Furthermore, we observe a connection between faster establishment of the maximum leakage level (Figure 2) and a higher relative increase in tryptophan emission intensity (Figure 9), suggesting that peptide penetration into the hydrocarbon core is a prerequisite for efficient leakage. On the other hand, we do not find any correlation between ordered or disordered peptide binding and leakage efficiency; both alternatives result in high leakage levels. To be able to judge the mode of action by which these peptides cause leakage, i.e., by "carpet" or "detergent" mechanisms, a dedicated leakage study would be required.

CONCLUSIONS

The influenza virus fusion peptide HA2(1−23) and its mutated glutamic acid-enriched version INF7 induce high degrees of leakage in both zwitterionic and slightly acidic LUVs. This study shows that INF7 displays pH-sensitive characteristics promising potential future use in peptide-based drug delivery systems, whereas HA2(1−23) is, expectedly, too active at pH 7.4. The origin of pH sensitivity seems related to the fact that INF7, with five negative charges at pH 7.4, is hindered from deep penetration into the membrane hydrocarbon core under physiological conditions. In addition, there is a possible correlation between induced membrane lipid disorder, measured using the membrane probe retinoic acid, and leakage capacity. From LD we conclude that HA2 peptides display poor alignment in zwitterionic LUV membranes, compared to slightly acidic LUVs. We also present evidence for slow changes (hours) in peptide−lipid interactions, resulting in reduced lipid order and in most cases more efficient shielding of tryptophans, not related to the fast initial peptide-induced membrane leakage of small dyes.

Using linear dichroism spectroscopy, we have been able to show that HA2(1−23) in slightly acidic lipid membranes (POPC/POPG (4:1)) exhibits a high degree of orientation and that details regarding the binding geometry can be concluded from the orientations of the transition moments of the peptide backbone and of the aromatic side chains. HA2(1−23) displays few pH-sensitive characteristics under the experimental conditions of our study. This can be understood from the limited conformational change we propose for this peptide upon reduction of pH from 7.4 to 5.0. We suggest, on the basis of the LD features of Tyr22, that the positioning of the peptide C-terminus is driven by interfacial interactions of Tyr22 and Trp23; this positioning is insensitive to pH. Furthermore, no change in oblique insertion of the peptide backbone is observed, suggesting that the pH-induced conformational change is primarily due to minor rearrangement of the peptide backbone in the hinge region around Trp14. LD of INF7 at pH 7.4 is different from that of HA2(1−23) and suggests a more surface-oriented binding mode, perhaps providing an explanation of its pH sensitivity. Due to the fact that INF7 displays poor membrane orientation at pH 5.0, informative information on the relation between structure and leakage-inducing capacity could not be obtained, but it can safely be concluded that INF7, due to the glutamic acid residues at positions 4 and 7, interacts with lipid membranes rather differently than HA2(1−23).

ACKNOWLEDGMENT

Marie Sjöberg at Astra Zeneca R&D in Mölndal is thanked for allowing us access to the osmometer.

REFERENCES

1. *Handbook of Cell-penetrating Peptides* (2007) 2nd ed., CRC Press, Taylor & Francis Group, Boca Raton, FL, London, New York.
2. Fischer, R., Fotin-Mleczek, M., Hufnagel, H., and Brock, R. (2005) Break on through to the other side-biophysics and cell biology shed light on cell-penetrating peptides, *ChemBioChem 6*, 2126−2142.
3. Thoren, P. E., Persson, D., Isakson, P., Goksor, M., Onfelt, A., and Norden, B. (2003) Uptake of analogs of penetratin, Tat(48−60) and oligoarginine in live cells, *Biochem. Biophys. Res. Commun. 307*, 100−107.
4. Zorko, M., and Langel, U. (2005) Cell-penetrating peptides: mechanism and kinetics of cargo delivery, *Adv. Drug Delivery Rev. 57*, 529−545.
5. Wadia, J. S., Stan, R. V., and Dowdy, S. F. (2004) Transducible TAT-HA fusogenic peptide enhances escape of TAT-fusion proteins after lipid raft macropinocytosis, *Nat. Med. 10*, 310−315.
6. Cho, Y. W., Kim, J. D., and Park, K. (2003) Polycation gene delivery systems: escape from endosomes to cytosol, *J. Pharm. Pharmacol. 55*, 721−734.
7. Tamm, L. K. (2003) Hypothesis: spring-loaded boomerang mechanism of influenza hemagglutinin-mediated membrane fusion, *Biochim. Biophys. Acta 1614*, 14−23.
8. Chang, D. K., Cheng, S. F., Lin, C. H., Kantchev, E. B., and Wu, C. W. (2005) Self-association of glutamic acid-rich fusion peptide analogs of influenza hemagglutinin in the membrane-mimic environments: effects of positional difference of glutamic acids on side chain ionization constant and intra- and inter-peptide interactions deduced from NMR and gel electrophoresis measurements, *Biochim. Biophys. Acta 1712*, 37−51.

9. Plank, C., Oberhauser, B., Mechtler, K., Koch, C., and Wagner, E. (1994) The influence of endosome-disruptive peptides on gene transfer using synthetic virus-like gene transfer systems, *J. Biol. Chem. 269*, 12918−12924.
10. Han, X., Bushweller, J. H., Cafiso, D. S., and Tamm, L. K. (2001) Membrane structure and fusion-triggering conformational change of the fusion domain from influenza hemagglutinin, *Nat. Struct. Biol. 8*, 715−720.
11. Luneberg, J., Martin, I., Nussler, F., Ruysschaert, J. M., and Herrmann, A. (1995) Structure and topology of the influenza virus fusion peptide in lipid bilayers, *J. Biol. Chem. 270*, 27606−27614.
12. Lai, A. L., Park, H., White, J. M., and Tamm, L. K. (2006) Fusion peptide of influenza hemagglutinin requires a fixed angle boomerang structure for activity, *J. Biol. Chem. 281*, 5760−5770.
13. Hsu, C. H., Wu, S. H., Chang, D. K., and Chen, C. (2002) Structural characterizations of fusion peptide analogs of influenza virus hemagglutinin. Implication of the necessity of a helix-hinge-helix motif in fusion activity, *J. Biol. Chem. 277*, 22725−22733.
14. Wharton, S. A., Martin, S. R., Ruigrok, R. W., Skehel, J. J., and Wiley, D. C. (1988) Membrane fusion by peptide analogues of influenza virus haemagglutinin, *J. Gen. Virol. 69* (Part 8), 1847−1857.
15. Wu, C. W., Cheng, S. F., Huang, W. N., Trivedi, V. D., Veeramuthu, B., Assen, B. K., Wu, W. G., and Chang, D. K. (2003) Effects of alterations of the amino-terminal glycine of influenza hemagglutinin fusion peptide on its structure, organization and membrane interactions, *Biochim. Biophys. Acta 1612*, 41−51.
16. Chen, Y. H., Yang, J. T., and Chau, K. H. (1974) Determination of helix and beta-form of proteins in aqueous-solution by circular-dichroism, *Biochemistry 13*, 3350−3359.
17. Ardhammar, M., Mikati, N., and Norden, B. (1998) Chromophore orientation in liposome membranes probed with flow dichroism, *J. Am. Chem. Soc. 120*, 9957−9958.
18. Norden, B., Kubista, M., and Kurucsev, T. (1992) Linear dichroism spectroscopy of nucleic-acids, *Q. Rev. Biophys. 25*, 51−170.
19. Ardhammar, M., Lincoln, P., and Norden, B. (2002) Invisible liposomes: refractive index matching with sucrose enables flow dichroism assessment of peptide orientation in lipid vesicle membrane, *Proc. Natl. Acad. Sci. U.S.A. 99*, 15313−15317.
20. Caesar, C. E., Esbjorner, E. K., Lincoln, P., and Norden, B. (2006) Membrane interactions of cell-penetrating peptides probed by tryptophan fluorescence and dichroism techniques: correlations of structure to cellular uptake, *Biochemistry 45*, 7682−7692.
21. Svensson, F. R., Lincoln, P., Norden, B., and Esbjorner, E. K. (2007) Retinoid chromophores as probes of membrane lipid order, *J. Phys. Chem. B.* (in press).
22. Brahms, J., Pilet, J., Damany, H., and Chandrasekharan, V. (1968) Application of a new modulation method for linear dichroism studies of oriented biopolymers in the vacuum ultraviolet, *Proc. Natl. Acad. Sci. U.S.A. 60*, 1130−1137.
23. Cantor, C. R., and Schimmel, P. R. (1980) *Biophysical Chemistry Part II: Techniques for the study of biological structure and function*, W. H. Freeman and Co., San Francisco.
24. Rodger, A., and Norden, B. (1997) *Circular Dichroism and Linear Dichroism*, Oxford University Press, Oxford, U.K.
25. Albinsson, B., and Norden, B. (1992) Excited-state properties of the indole chromophore: Electronic transition moment directions from linear dichroism measurements: Effect of methyl and methoxy substituents, *J. Phys. Chem. 96*, 6204−6212.
26. Lakowicz, J. R. (1999) *Principles of Fluorescence Spectroscopy*, 2nd ed., Kluwer Academic/Plenum Publishers, New York.
27. Rosenheck, K., and Doty, P. (1961) The far ultraviolet absorption spectra of polypeptide and protein solutions and their dependence on conformation, *Proc. Natl. Acad. Sci. U.S.A. 47*, 1775−1785.
28. Ladokhin, A. S., Wimley, W. C., Hristova, K., and White, S. H. (1997) Mechanism of leakage of contents of membrane vesicles determined by fluorescence requenching, *Methods Enzymol. 278*, 474−486.
29. Lear, J. D., and DeGrado, W. F. (1987) Membrane binding and conformational properties of peptides representing the NH2 terminus of influenza HA-2, *J. Biol. Chem. 262*, 6500−6505.
30. Brattwall, C. E., Lincoln, P., and Norden, B. (2003) Orientation and conformation of cell-penetrating peptide penetratin in phospholipid vesicle membranes determined by polarized-light spectroscopy, *J. Am. Chem. Soc. 125*, 14214−14215.
31. Esbjorner, E. K., Caesar, C. E., Albinsson, B., Lincoln, P., and Norden, B. (2007) Tryptophan orientation in model lipid membranes, *Biochem. Biophys. Res. Commun. 361*, 645−650.
32. Persson, D., Thoren, P. E., and Norden, B. (2001) Penetratin-induced aggregation and subsequent dissociation of negatively charged phospholipid vesicles, *FEBS Lett. 505*, 307−312.
33. Beschiaschvili, G., and Seelig, J. (1991) Peptide binding to lipid membranes. Spectroscopic studies on the insertion of a cyclic somatostatin analog into phospholipid bilayers, *Biochim. Biophys. Acta 1061*, 78−84.
34. Chang, D. K., Cheng, S. F., Deo Trivedi, V., and Yang, S. H. (2000) The amino-terminal region of the fusion peptide of influenza virus hemagglutinin HA2 inserts into sodium dodecyl sulfate micelle with residues 16−18 at the aqueous boundary at acidic pH. Oligomerization and the conformational flexibility, *J. Biol. Chem. 275*, 19150−19158.
35. Durrer, P., Galli, C., Hoenke, S., Corti, C., Gluck, R., Vorherr, T., and Brunner, J. (1996) H+-induced Membrane Insertion of Influenza Virus Hemagglutinin Involves the HA2 Amino-terminal Fusion Peptide but Not the Coiled Coil Region, *J. Biol. Chem. 271*, 13417−13421.
36. Nobusawa, E., Hishida, R., Murata, M., Kawasaki, K., Ohnishi, S., and Nakajima, K. (1995) The role of acidic residues in the "fusion segment" of influenza A virus hemagglutinin in low-pH-dependent membrane fusion, *Arch. Virol. 140*, 865−875.
37. Steinman, R. M., Mellman, I. S., Muller, W. A., and Cohn, Z. A. (1983) Endocytosis and the recycling of plasma membrane, *J. Cell Biol. 96*, 1−27.
38. Yau, W. M., Wimley, W. C., Gawrisch, K., and White, S. H. (1998) The preference of tryptophan for membrane interfaces, *Biochemistry 37*, 14713−14718.
39. Vaccaro, L., Cross, K. J., Kleinjung, J., Straus, S. K., Thomas, D. J., Wharton, S. A., Skehel, J. J., and Fraternali, F. (2005) Plasticity of influenza haemagglutinin fusion peptides and their interaction with lipid bilayers, *Biophys. J. 88*, 25−36.
40. Persson, D., Thoren, P. E., Herner, M., Lincoln, P., and Norden, B. (2003) Application of a novel analysis to measure the binding of the membrane-translocating peptide penetratin to negatively charged liposomes, *Biochemistry 42*, 421−429.
41. Wimley, W. C., and White, S. H. (1996) Experimentally determined hydrophobicity scale for proteins at membrane interfaces, *Nat. Struct. Biol. 3*, 842−848.
42. Jaysinghe, S., Hristova, K., Wimley, W. C., Snider, C., and White, S. H. (2006) Membrane Protein Explorer (MPEx), http://blanco.biomol.uci.edu/mpex.
43. Wimley, W. C., Creamer, T. P., and White, S. H. (1996) Solvation energies of amino acid side chains and backbone in a family of host-guest pentapeptides, *Biochemistry 35*, 5109−5124.
44. Dubovskii, P. V., Li, H., Takahashi, S., Arseniev, A. S., and Akasaka, K. (2000) Structure of an analog of fusion peptide from hemagglutinin, *Protein Sci. 9*, 786−798.
45. Cheng, S. F., Kantchev, A. B., and Chang, D. K. (2003) Fluorescence evidence for a loose self-assembly of the fusion peptide of influenza virus HA2 in the lipid bilayer, *Mol. Membr. Biol. 20*, 345−351.
46. Han, X., and Tamm, L. K. (2000) pH-dependent self-association of influenza hemagglutinin fusion peptides in lipid bilayers, *J. Mol. Biol. 304*, 953−965.

BI701075Y